



26 ones. This confirms that the requirement for the important factor maps can be assessed based
27 on the physiography of the region. Based on the analysis of the three models, it was observed
28 that most commonly available feature data can be useful for carrying out LSM at regional scale,
29 eliminating the least available ones in most of the use cases due to data scarcity. Identifying
30 LSMs at regional scale has implications for understanding landslide phenomena in the region
31 and post-event relief measures, planning disaster risk reduction, mitigation, and evaluating
32 potentially affected areas.

33

34 1. Introduction

35

36 Landslides are one of the most frequently occurring natural disasters that cause significant
37 human casualties and infrastructure destruction. Landslides are triggered by several natural and
38 man-made triggering events such as earthquakes, volcanic eruptions, heavy rains, extreme
39 winds, and unsustainable construction activities such as informal settlement development and
40 cutting of roads along the slopes (Glade et al., 2006; van Westen et al., 2008). Extreme
41 meteorological events such as the Vaia storm of 2018 triggered landslides and debris flow,
42 destroyed critical infrastructures in the northern parts of Italy (Boretto et al., 2021). As reported
43 by (Gariano et al., 2021) in the last 50 years between 1969-2018, landslides posed a severe
44 threat to the Italian population. Approximately, 1500 out of the 8100 municipalities in Italy
45 have faced landslides with severe fatalities. Between the years of 1990 and 1999, 263 people
46 were killed by landslides. Studies by (Rossi et al., 2019) estimated that approximately 2500
47 people were killed between 1945-1990. Moreover, predictive modelling of the Italian
48 population at risk to landslides (Rossi et al., 2019) shows massive tendency of risk to the
49 population with data acquired between 1861-2015, emphasizing the necessity of landslide risk
50 studies.



51 Therefore, to assess landslide risk and plan for suitable risk mitigation measures, it is crucial
52 to realize the significance of landslide studies, particularly landslide susceptibility mapping
53 (LSM). LSM is an essential tool that incorporates the potential landslide locations (Senouci et
54 al., 2021). The probability of a landslide occurring in a particular region owing to the effects
55 of several causative factors is referred to as landslide susceptibility. LSM is an essential step
56 towards landslide risk management and helps in effective mapping of the spatial distribution
57 of probable landslide manifestations (Dai et al., 2002). In the past, researchers have used a
58 range of models to assess landslide susceptibility using technologies such as Earth Observation
59 (EO) and Geographic Information Systems (GIS). The extraction and analysis of slope
60 movements have been going on since the early 1970s (Brabb et al., 1972) and is still one of the
61 most important tools to perform LSM (Castellanos Abella and Van Westen, 2008; Catani et al.,
62 2013; Chacón et al., 2006; Ercanoglu and Gokceoglu, 2002; Floris et al., 2011; Guzzetti et al.,
63 2006; Liu et al., 2021; Pham et al., 2015; Reichenbach et al., 2018; Youssef and Pourghasemi,
64 2021).

65

66 Traditional methods such as the expert-based Analytical Hierarchy Process (AHP), multi-
67 variate statistics, data-driven Frequency Ratio (FR) have been employed for landslide
68 susceptibility for many years, with satisfactory results (Castellanos Abella and Van Westen,
69 2008; Komac, 2006; Pradhan, 2010). Examples of such approaches is given in the study area,
70 by Floris et al. (2011) which combined traditional LSM methods with an updated online
71 landslide database in the Veneto Region, Italy, where they used online spatial data from Italian
72 portals for mapping landslide susceptibility at medium and large scales. Afterwards, with the
73 development of new approaches, susceptibility modelling has advanced from traditional
74 approaches. Presently, two approaches: (1) statistical and (2) machine learning, are practised
75 for LSM at investigating the landslide predisposing factors and to map the geographical



76 distribution of landslide processes. Reichenbach et al., (2018) classified landslide susceptibility
77 models into six main groups: (1) classical statistics, (2) index-based, (3) machine learning, (4)
78 multi-criteria analysis, (5) neural networks, and (6) others. Research by (Reichenbach et al.,
79 2018) also depicted that before 1995, only five models were used for LSM, but in recent times,
80 an investigation of 19 other models was carried out, which yielded good results. More than 50
81 per cent of the methods consisting of the first five models mentioned above accounted for
82 landslide susceptibility studies. Recent work of (Stanley et al., 2021) emphasized the
83 importance of data-driven methods in global LSM, trained to report landslide spatial
84 occurrences between the periods of 2015-2018. The first version of the Landslide Hazard
85 Assessment for Situational Awareness (LHASA) from their work for NASA, reported landslide
86 occurrences with a decision tree model that first defines the intensity of one week of rainfall.
87 LHASA version 2 used the data-driven model of XG-Boost by adding two dynamically varying
88 factors: snow and soil moisture. However, despite advances in LSM, the advent of feature
89 importance or the importance of the causative factors in the prediction capability of a model is
90 not discussed enough. The need of increasing our control over the model sensitivity to system
91 parameters changes, including those induced by anthropogenic and climate-change dynamics,
92 is becoming a key factor in the implementation of truly efficient LSM for risk mitigation
93 purposes. The VAIA windstorm of 2018, as a typical extreme weather event, may easily escape
94 traditional statistical prediction schemes and represent, therefore, a challenging test for
95 exploring the sensitivity of the various LSM models to changing factors and conditions.

96
97 One goal of this research is to look into the relative changes in LSM accuracy when the least
98 "important" conditioning factors are removed. Feature selection in LSM is an approach in
99 reducing landslide conditioning features to improve model performance and reduce
100 computational costs. The purpose of this approach is to find the optimal set of conditioning



101 features that will provide the best fit for the model to yield higher accuracy as predictions.
102 Micheletti et al., (2014) emphasized the importance of feature selection in LSM and discussed
103 the use of Machine Learning (ML) models such as Support Vector Machine (SVM), Random
104 Forest (RF), and AdaBoost for LSM, as well as the significance of associated features within
105 the confluence of the ML models for feature importance. However, their study did not consider
106 geological and meteorological features like lithology, land use, and rainfall intensity for both
107 LSM and feature selection. Studies by Liu et al., (2021) depicted the improvement in the
108 predictive capability of the so-called Feature Selected Machine Learning (FS-ML) model but
109 also remarked on the fact that the same features may contribute differently in different ML
110 models. In this study, we wanted to investigate post-prediction feature selection approach to
111 improve LSM accuracy in contrast to what has been done in literature like Liu et al., (2021),
112 where they perform pre-prediction feature importance using approaches like multi-collinearity
113 analysis, variance inflation factor. The identification of the most crucial features can help in
114 monitoring the effect of extreme events (such as Vaia) on the increase of landslide hazard. This
115 has implications for observation of the influence of extreme events on crucial factors in
116 comprehending the changes in the evolution of hazard can be evaluated.

117 We present a study in the province of Belluno, northern Italy, with the comparison of feature
118 or factor importance of statistical and ML models for LSM before the Vaia storm event. The
119 results from the LSM will be then validated using the IFFI landslide inventory data for testing
120 the various models' prediction capability with/without certain factors. We also investigate
121 whether many of the latter features are crucial for LSM. As in many regions over the world,
122 the same data or factor maps might not be available.

123

124 2. Study area and Data

125 2.1 Study area



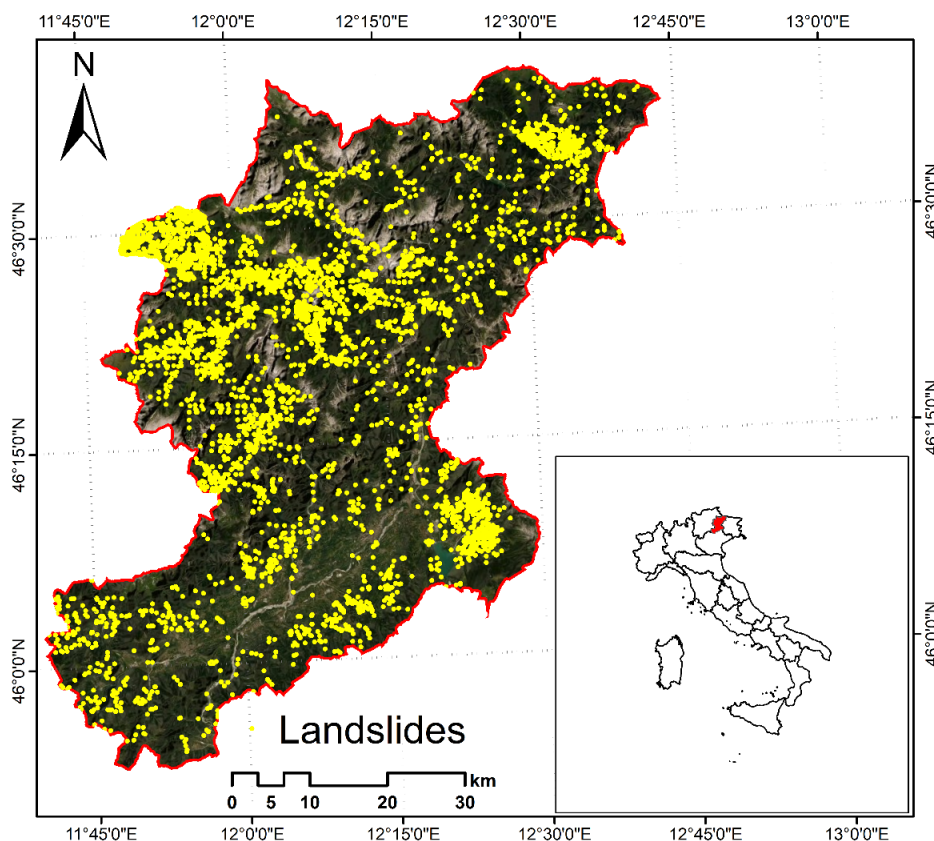
126 The area of the Belluno Province (Veneto Region, NE Italy) is part of the tectonic unit of the
127 Southern Alps. The territory is 3,672 km² wide, stretching from north to south between the
128 Dolomite Alps and the Venetian Pre-Alps, with elevations ranging from 42 to 3325 m above
129 mean sea level. From a geological point of view, Dolomite Alps comprises the Hercynian
130 crystalline basement consisting of micaschists and phyllites intruded by the Permian
131 ignimbrites (Doglioni, 1990; Schönborn, 1999) These Paleozoic units are mainly outcropping
132 in the NE and central-West sectors. The Middle-Upper Triassic includes carbonate, volcanic
133 and dolomitic formations. In particular, the Upper Triassic Main Dolomite covers 14% of the
134 whole province. Jurassic-Cretaceous limestone and marls are especially located between the
135 Valsugana and Belluno thrusts (Sauro et al., 2013). Moreover, in the Belluno valley and in the
136 southern part of the area, Cenozoic sediments, i.e., flysch and molasse and Quaternary glacial,
137 alluvial and colluvial deposits are largely present. Instead, Venetian Prealps are characterized
138 by Jurassic-Cretaceous sedimentary cover, such as layered limestones and dolomites with
139 cherts (Compagnoni et al., 2005; Corò et al., 2015). Because of its morphological
140 characteristics, the study area is affected by slope instability, which overlay an area of 165 km²
141 corresponding to 6% of the province (Baglioni et al., 2006). Most of the landslide phenomena
142 are located in the NW (Upper basin of Cordevole River) and SE (Alpago district) sectors of the
143 province (Figure 1). The dominant landslide types are slides (47%), rapid flows (20%), slow
144 flows (12%), and shallow soil slips (7%) (Iadanza et al., 2021). The climate of the province of
145 Belluno is continental. The mean annual temperature recorded in the period 1961–1990 is 7°C
146 and the mean precipitation is 1284 mm/year (Desiato et al., 2005) with two peaks distributed
147 in spring and autumn. In the last 27 years, temperature and rainfall intensity in the study area
148 have increased due to climatic changes leading to more frequent meteorological conditions
149 ARPAV (Agenzia Regionale per la Prevenzione e Protezione Ambientale del Veneto).

150



151 2.2 Landslide inventory data

152 The inventory of landslide phenomena in Italy (IFFI) conducted by the Italian Institute for
153 Environmental Protection and Research (ISPRA) and the Regions and Autonomous Provinces
154 was used in this study (Trigila et al., 2010). The IFFI Project was financed in 1997. Since 2005,
155 the catalogue is available online and consists of point features indicating the scarp of the
156 landslides and polygon features delineating the instabilities. The archive stores the main
157 attributes of the landslides, such as morphometry, type of movement, rate, involved material,
158 induced damages and mitigation measures. The inventory currently holds 620,808 landslides
159 collected from historical documents, field surveys and aerial photointerpretation, covering an
160 area of 23,700 km², which corresponds to the 7.9% of the Italian territory (Trigila and Iadanza,
161 2018). In the Belluno province, the IFFI inventory consists of 5934 points of landslides
162 occurred before 2006 (Baglioni et al., 2006).



164 Figure 1: Location of the study area and landslides (yellow points) collected by IFFI
165 (Inventory of Landslide Phenomena in Italy) project.

166

167 2.3 Landslide conditioning factors

168 Based on the regional environmental characteristics of the study area and the scientific
169 literature, fourteen landslide conditioning factors were selected, including: (i) topographical
170 factors such as elevation, slope angle, slope aspect, topographical wetness index (TWI),
171 topographical position index (TPI), topographical roughness index (TRI), profile curvature,
172 and plan curvature; (ii) hydrological factors (i.e., distance to drainage, precipitation);
173 geological factors (lithology); (iii) anthropogenic factors (distance to roads); and (iv)
174 environmental factors like Normalized Difference Vegetation Index (NDVI) and landcover



175 (see figure 2). A freely accessible digital elevation model (DEM) with a spatial resolution of
176 25 metres was downloaded from the Veneto Region cartographic portal
177 (<https://idt2.regione.veneto.it>), was used to derive the topographical layers. Refer to table 1 for
178 a detailed description of the conditioning factors. Land cover, lithology maps, road network
179 and drainage maps were downloaded from the same portal. Rainfall data was downloaded from
180 the Regional Agency for the Environmental Prevention and Protection of Veneto (ARPAV:
181 <https://www.arpa.veneto.it/>) web site.

182

183

184

185 Table 1: Description of the conditioning factors for landslide occurrences.

186

Sl No.	Conditioning Factor	Data Range	Description/Justification
1	Elevation	42 m to 3325 m	The geomorphological and geological processes are affected by elevation (Raja et al., 2017). It has an impact on topographic characteristics, which contribute to spatial differences in many landform processes, as well as the distribution of vegetation.
2	Slope	Flat areas to very high slopes till 86.48°	Slope is a derivative of the DEM which can cause failure of slope (Pham et al., 2018). Landforms having a higher angle of slope are usually more susceptible to collapse, which is closely correlated to landslides.



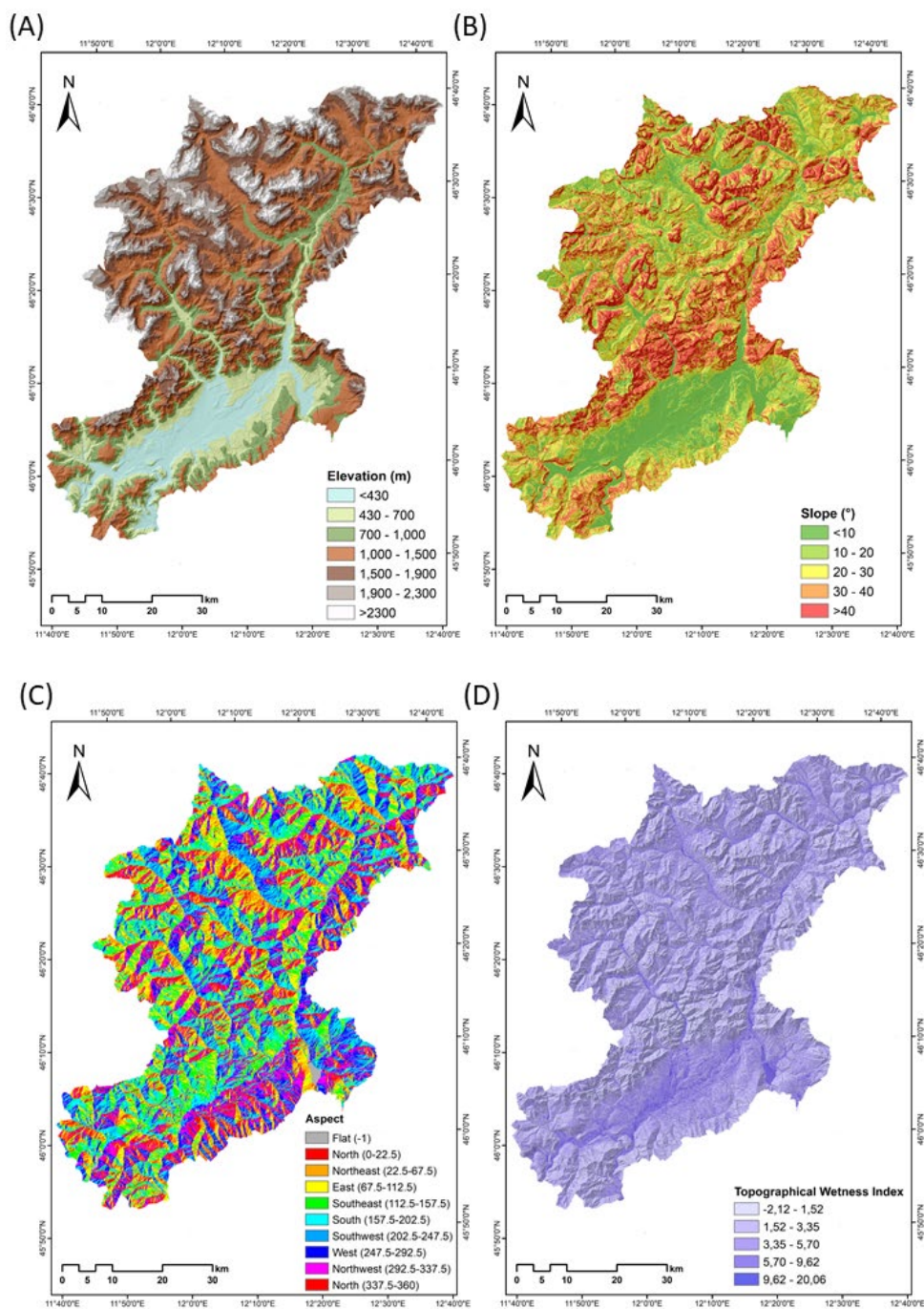
3	Aspect	North (0 degrees) to North (360 degrees)	Aspect has a correlation with other geo-environmental factors is a crucial factor for LSM that describes the slope direction (Dahal et al., 2008). The slope direction to a degree dictates the frequency of landslides.
4	Topographic wetness index	-2.12 to 20.06	The influence of topography on the location and amount of saturated runoff source areas is an essential conditioning factor (Pourghasemi et al., 2012). TWI measures the amount of accumulated water and distribution of soil moisture at a location. Higher TWI values can relate to higher chances of landslide occurrence.
5	Topographic Position Index	-1143.68 to 243.84	The topographic position index (TPI) shows the difference between the elevation of a point and its surrounding defined by a specified radius. Lower values represents the plausibility of features lower than the surrounding, thus possibly relating to higher odds of landslide occurrence.
6	Topographic Roughness Index	0 to 1077.30	Topographic Roughness Index (TRI) calculates the difference in elevation between adjacent pixels in a DEM which depicts the terrain fluctuation (Riley et al., 1999). As the slope of a landscape moves, the TRI decreases, relating to slope movement.

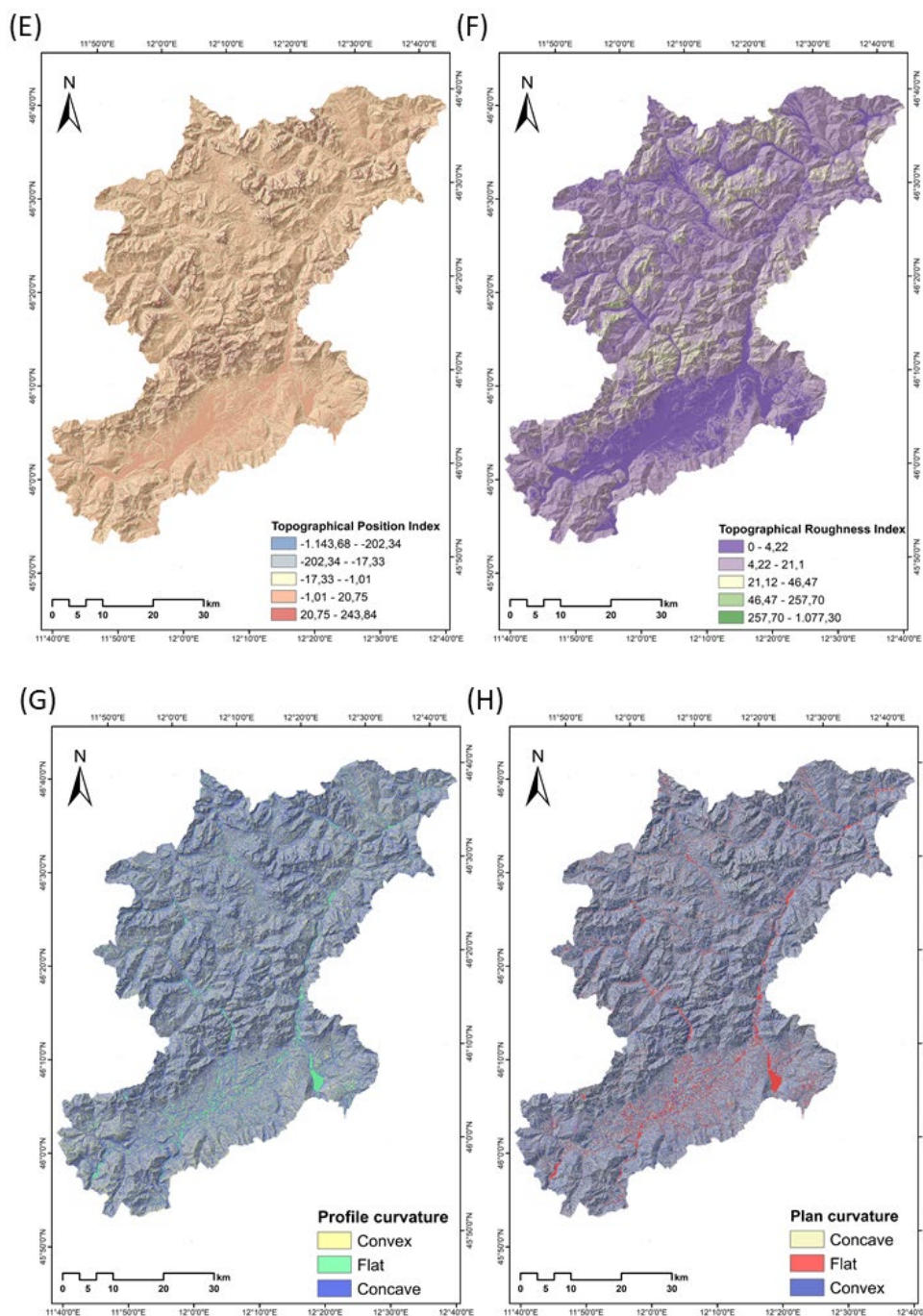


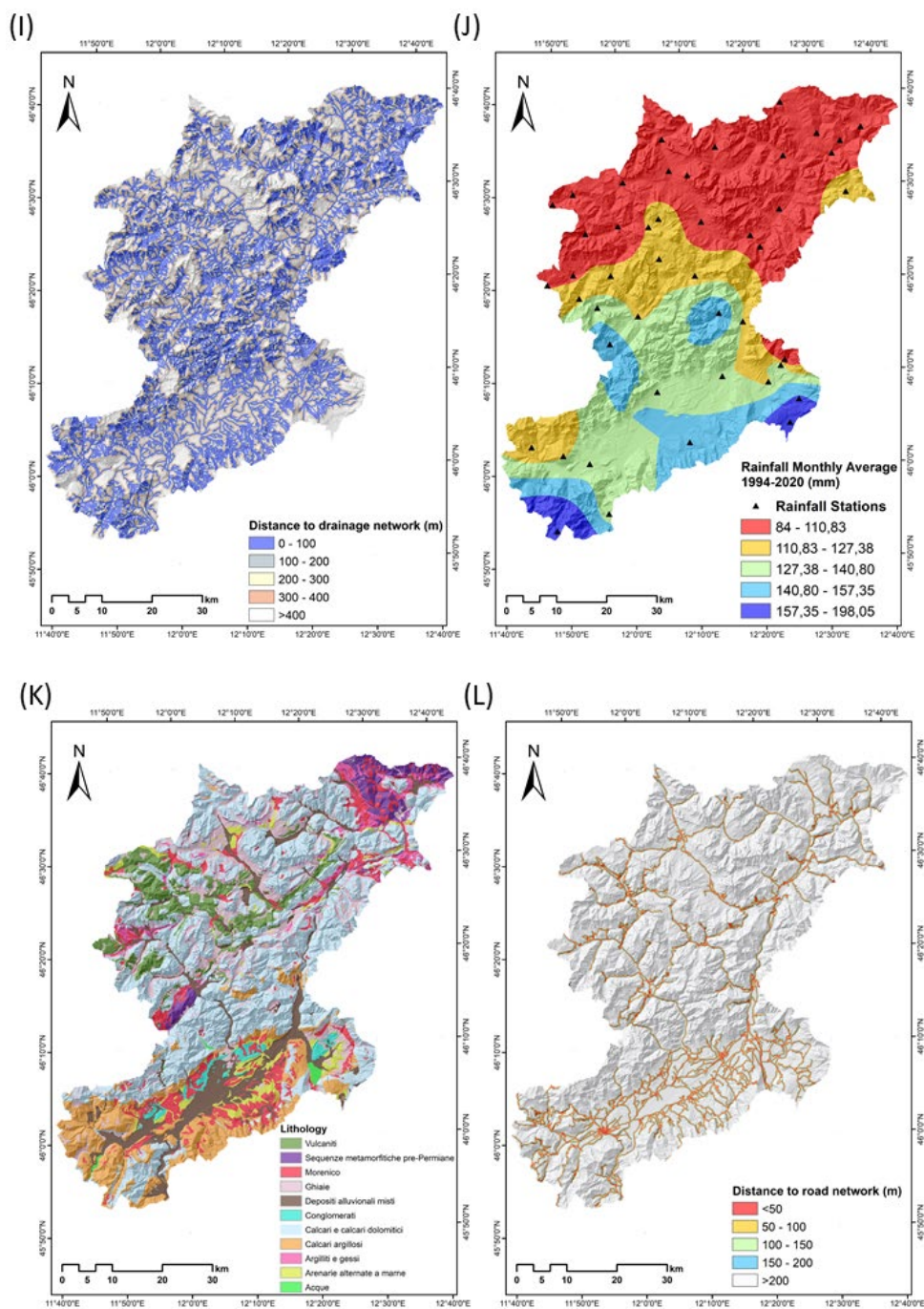
7	Profile Curvature	Concave Flat Convex	The driving and resisting forces within a landslide in the slope direction are affected by profile curvature.
8	Plan Curvature	Concave Flat Convex	The direction of landslide movement is controlled by the plan curvature, which regulates the convergence or divergence of landslide material (Dury, 1972; Meten et al., 2015).
9	Drainage	0 to 400	Drainage transports water, which induces material saturation, culminating in landslides in valleys. (Shahabi and Hashim, 2015).
10	Rainfall	84 to 1198.05 (mm/month)	Precipitation characteristics shift by climatic conditions and geographical characteristics, resulting in significant temporal and geographical variations in rainfall quantity and intensity. This can lead to the triggering of landslides across large areas but also for specific smaller areas.
11	Lithology	Volcanites, Pre-Permian, metamorphic, sequence Morainic, Gravels, etc.	The geological strength indices, failure susceptibility, and permeability of lithological units differ (Yalcin and Bulut 2006), where changes in the stress-strain behaviour of the rock strata can be caused by lithological unit variation. Slope failure typically occurs on a slope with low strength and permeability.

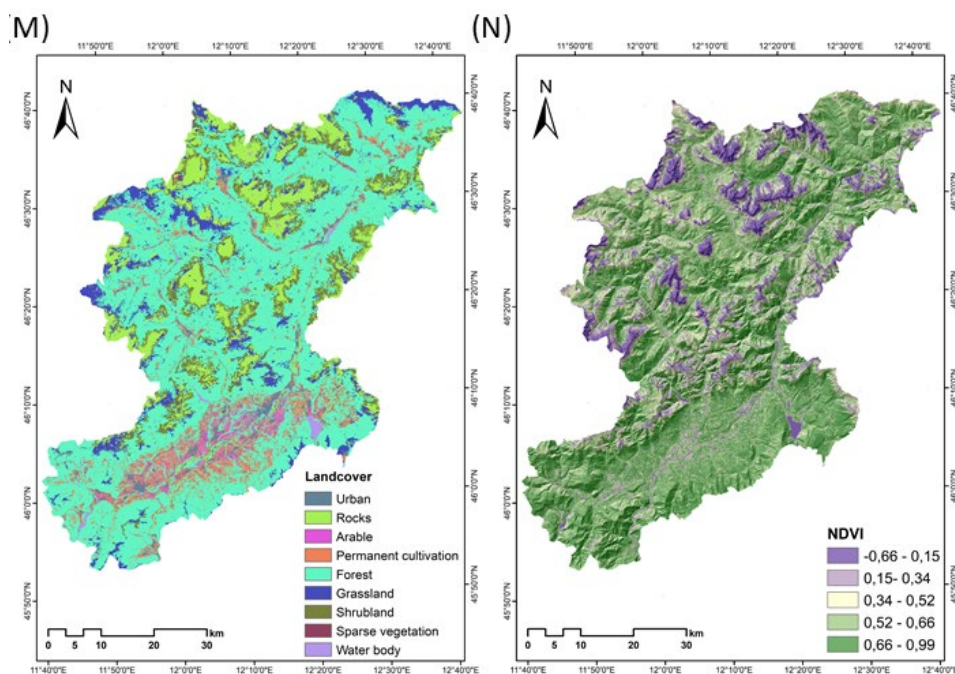


12	Distance to Roads	0 to 200	A crucial manmade element impacting the occurrence of landslides is roads because of road clear-cutting and construction activities (Dunning et al., 2009).
13	Landcover	Rock, Forest, Urban cover etc.	Land cover can be utilized to describe the region's vastly dismembered zones and the likelihood of landslide activities.
14	NDVI	-0.66 to 0.66	NDVI is important in realizing the amount of vegetation cover which can be interpreted to understand the strength of the slope and the landslide occurrences. The NDVI reflects the inhibitory effect of landslide occurrence (Huang et al., 2020).









192

193 Figure 2: Maps of the conditioning factors used in this study: (A) Elevation, (B) Slope, (C)
194 Aspect, (D) Topographical wetness index, (E) Topographical position index, (F) Topographical
195 roughness index, (G) Profile curvature, (H) Plane curvature, (I) Distance to drainage networks,
196 (J) Rainfall monthly average (1994-2020) mm, (K) Lithology, (L) Distance to road network
197 (M) Landcover, (N) NDVI

198

199 3. Methodology

200

201 We propose an approach that help understand the intrinsic relationship between the features
202 and the output post-prediction, which can be then refined by removing the less "important"
203 features throughout the statistical and ML models. As stated previously, the study attempts the
204 application of sensitivity analysis to understand relative feature importance as a preliminary



205 step towards the modelling of a space-time changing parameter in LSM methods. The apparent
206 reality is not as simple as using a certain model that gives the highest LSM accuracy and using
207 said derived outputs maps for disaster risk management and mitigation measures. Therefore, It
208 is important to test the effects of the features and it's relative importance in LSM. The
209 successive sub-sections address the definitions of the statistical and ML models for LSM.

210

211 3.1 Statistical approach

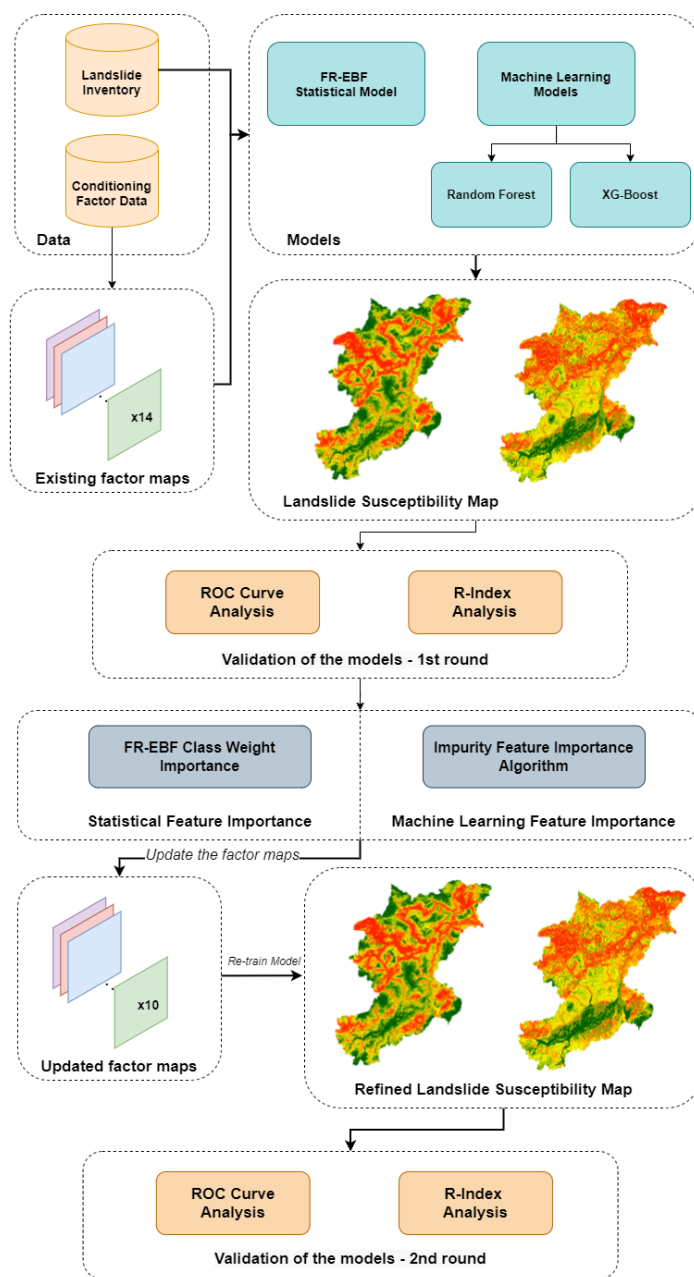
212 3.1.1 Ensemble Frequency Ratio - Evidence Belief Function

213

214 In landslide susceptibility studies, the frequency ratio (FR) model is often applied. This is a
215 straightforward evaluation tool which calculates the likelihood of landslide occurrence and
216 non-occurrence for each conditioning factor. (Lee, 2013; Mondal and Maiti, 2013; Shahabi et
217 al., 2014). For each landslide, the FR is a probabilistic model based on observed correlations
218 between landslide distribution and related parameters (Lea Tien Tay 2014). The model depicts
219 the relationship between spatial locations and the factors that determine the occurrence of
220 landslides in a specific area. Spatial phenomenon and factor classes correlation can be found
221 through FR and is very helpful for geospatial analysis (Mahalingam et al. 2016; Meena et al.
222 2019b). Figure 3 gives an overview of the methodology employed in this study.

223 The proportion of landslide inventory points for all classes within each factor can be used to
224 compute FR weights. The area ratio for each of the factor classes in relation to the total area of
225 the study region was calculated by overlapping the landslide inventory points with the
226 conditioning factors. The FR weights are calculated by dividing the landslide occurrence ratio
227 in a class by the entire area in that class (Demir et al. 2012).

228



230

231 Figure 3: Overview of the conceptual workflow of methodology for landslide susceptibility

232

assessment.



233 Using the equation, the landslide susceptibility index (LSI) was computed by summing the
234 values of each factor ratio (Lee, 2013):

235

$$236 \quad \text{LSI} = \sum \text{FR} \quad (\text{Eq.2})$$

237

238 $\text{LSI} = (\text{DEM}) + (\text{slope}) + (\text{aspect}) + (\text{Topographic Wetness Index}) + (\text{Topographic Roughness}$
239 $\text{Index}) + (\text{Topographic Position Index}) + (\text{Distance to road}) + (\text{Distance to drainage}) + (\text{Land}$
240 $\text{Cover}) + (\text{Lithology}) + (\text{NDVI}) + (\text{Rainfall}) + (\text{Profile Curvature}) + (\text{Plain Curvature})$

241

242 Where the landslide susceptibility index is the LSI, and the frequency ratio of each factor type
243 is the FR. An FR value of 1 in the relationship analysis implies that the density of landslides in
244 a specific class is proportionate to the size of the class in the map; an LSI value of 1 is an
245 average value. Higher LSI values suggest a stronger correlation, whereas lower LSI values
246 imply a weaker correlation. In a nutshell, a greater LSI value represents higher landslide
247 susceptibility and the vice-versa. We integrated the LSI results with evidence belief functions
248 (EBF) derived predictor values. The EBF uses the conditioning factors defined by FR as the
249 input data. Eq. (3) was applied to the rating of every spatial factor with the training dataset.

250

$$251 \quad PR = \frac{SA_{max} - SA_{min}}{SA_{max} - SA_{min}} \min \quad (\text{Eq.3})$$

252

253 where SA is the indicator of spatial association (Bel) between spatial variables and landslides
254 and PR is the prediction rate. The lowest absolute difference of all variables is divided by the
255 computed absolute difference between the maximum and least SA values (Table 2). The
256 eigenvectors of the matrix were calculated by normalising each column's pairwise result. The
257 eigenvalue was calculated by dividing each pairwise importance rate in a column by the total

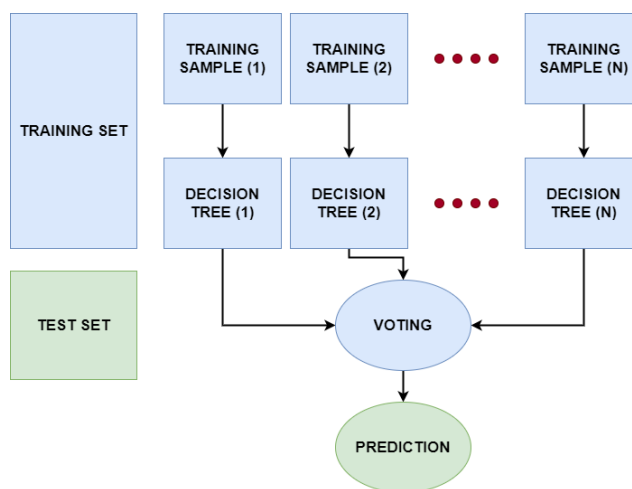


258 of the pairwise importance rates in that column. The fractional predictor is obtained by
259 averaging the eigenvectors across a row of matrices. Pairwise comparison of the PR values of
260 the slope failure predictors yielded the pairwise rating matrix of the predictor rating.

261 3.2 Machine learning models

262 3.2.1 Random Forest model

263 Random Forest (RF) is based on the fundamental concept of the "wisdom of crowds" where
264 multiple decision trees, introduced by (Breiman, 2001), has been utilized in a number of remote
265 sensing research for a variety of applications.(Melville et al., 2018). RF creates many deep
266 decision trees using the training data and it can overcome the overfitting problem mostly
267 resulting from complex datasets better than other decision trees. Each RF decision tree gives a
268 prediction, which is then weighted according to the value created from votes from each tree
269 (see figure 4). Since the RF has shown an impressive performance for classification purposes,
270 it is regarded as one of the most efficient non-parametric ensembles models (Chen et al., 2017).



272

273 Figure 4: Conceptual diagram of the Random Forest model.

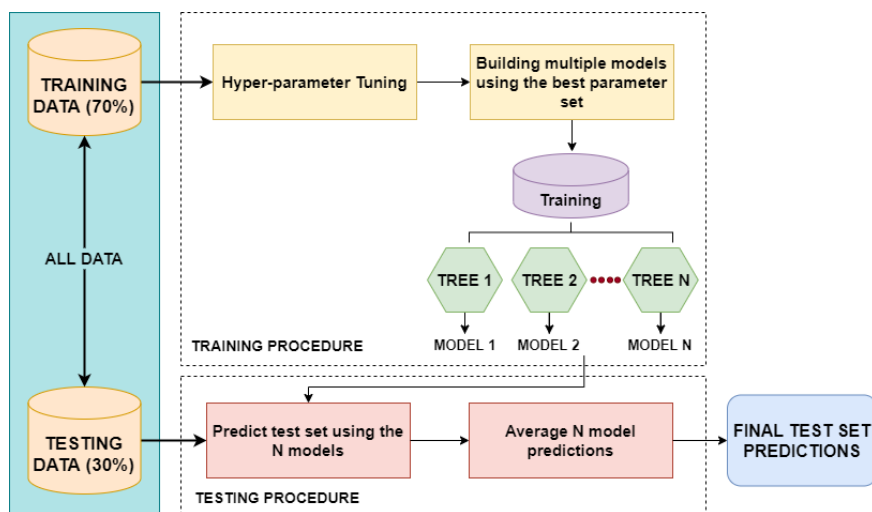
274

275 3.2.2 XG-Boost model



276 Extreme gradient boosting or commonly known as the XG-Boost ML model is an optimized
277 gradient boosting algorithm that is designed for optimum speed and performance and boosting
278 ensembles are used to generate a prediction model. (Sahin, 2020). The core idea of a boosting
279 algorithm is to combine the weaker learners to improve accuracy (Can et al., 2021). The model
280 is known for its fast-training speed for classification tasks. In the study, we use training
281 parameters to adjust the XG-Boost algorithm like learning rate, subsample ratio, maximum
282 depth of the tree and others. It uses boosting techniques to reduce overfitting problems to
283 improve accuracy results (figure 5).

284



286

287 Figure 5: Training and testing procedure of the XG-Boost model.

288 3.3 Feature selection algorithms

289 The goal of feature selection is to aid in the discovery of acceptable conditions for training the
290 models and to increase generalisability in landslide prediction. This selection help eliminate
291 the irrelevant (less important) conditioning factors to obtain optimal prediction accuracy
292 (Micheletti et al., 2014). For the statistical model, we used class weights obtained from



293 frequency ratio and used them as input for generating predictor rate from FR-EBF model which
294 gives the final weights of the conditioning factors. So, we used the predictor rate weights to
295 select the suitable features.

296

297 In terms of the feature importance for selecting the right set of features (or factors in this case)
298 for both RF and XG-Boost, we use the in-built impurity feature importance algorithm which is
299 performed on the training set. Based on the results as ranks of features sorted in a descending
300 order, the most important features will be selected to investigate the improvement of model
301 performance in terms of the accuracy obtained. Thus, we can comment on whether certain
302 factors are impactful in performing LSM with ML models. Besides, the comparison of the
303 resulting important features of the different models can be interpreted to highlight the
304 respective strengths of the models and allow drawing better conclusions towards the robustness
305 of the relevant features for landslide predictions.

306

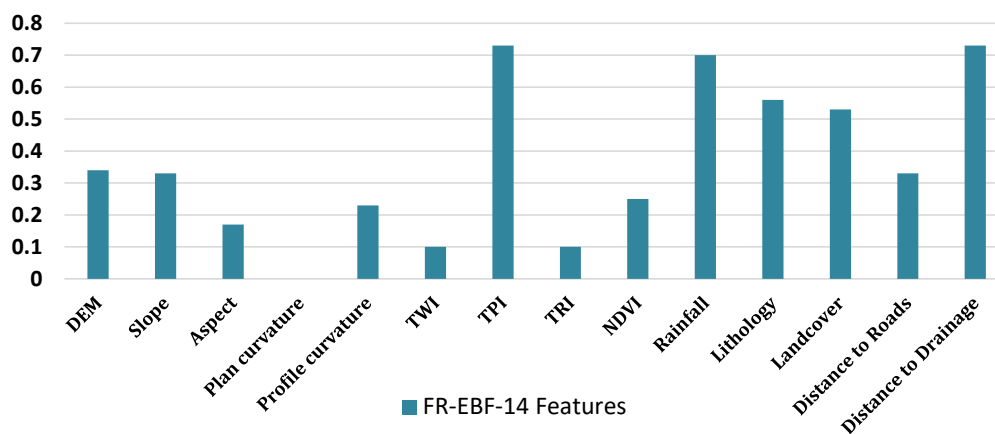
307 4. Results

308 4.1 Statistical model

309 The class weights were derived from data driven FR model and the final weights of the factors
310 were derived by using predictor rate from evidence belief function given in Table 2. The class
311 and factor weights were calculated using equations 1 and 2. The final weights of landslide
312 conditioning factors were calculated using an ensemble of FR-EBF, and then utilised to create
313 the final LSM. Because there is no common approach for identifying landslide susceptibility
314 classes in the final LSM, we normalised the findings to 0 to 100 for uniformity and
315 comparability. Using a quantile classification, which separates the values into groups with an
316 equal number of values, the resultant LSM was classified into five classes: very low, low,
317 moderate, high, and very high, as shown in figure 7.(Chung and Fabbri, 2003). This method of



318 classification gives a better distribution of values in each class than common approaches such
 319 as natural breaks, which can result in certain classes having limited or excessive data.
 320 In terms of the feature importance that we observe in figure 6 and Table 2 (normalized weights),
 321 based on the trial-and-error approach, factors (or features) under the threshold of 0.3 were
 322 discarded as they did not make much of a difference in terms of predicting landslide
 323 occurrences in the study area. Therefore, five conditioning factors having coefficient values
 324 lower than 0.30 were dropped and overall, the area under the curve (AUC) accuracy still
 325 remained similar to the original accuracy with the 14 factors.



326

327

328 Figure 6: Feature importance of the statistical model

329

330 Table 2: Frequency ratio values for spatial factors class weighting and EBF coefficients for
 331 predictor rates (PR) based on degrees of spatial associations.

332

Factors and classes	<i>Bel</i>	Min	Max	[Max-Min]	Predictor Rate	FR Weights	Normalized weights
Elevation		0.07	0.24	0.17	0.73		
<430	0.07					0.50	0.06



430 - 700	0.15			1.13	0.20
700 - 1000	0.13			0.96	0.19
1000 - 1500	0.12			0.86	0.15
1500 - 1900	0.11			0.81	0.12
1900 - 2300	0.24			1.72	0.17
>2300	0.18			1.31	0.12
<hr/>					
Profile		0.00	0.53	0.53	2.30
Curvature					
Concave	0.53			1.05	0.40
Flat	0.00			0.00	0.30
Convex	0.47			0.95	0.30
<hr/>					
Plan		0.00	0.52	0.52	2.26
Curvature					
Concave	0.52			1.03	0.35
Flat	0.00			0.00	0.33
Convex	0.48			0.97	0.32
<hr/>					
Slope		0.14	0.25	0.11	0.48
<10	0.14			0.70	0.14
10 - 20	0.23			1.11	0.22
20 - 30	0.25			1.25	0.27
30 - 40	0.20			0.99	0.20
>40	0.17			0.86	0.17
<hr/>					
Distance from		0.02	0.36	0.34	1.49
drainage					
0 - 100	0.36			1.15	0.28
100 - 200	0.30			0.97	0.19
200 - 300	0.23			0.74	0.12
300 - 400	0.10			0.31	0.07
>400	0.02			0.06	0.34



Distance from		0.08	0.24	0.15	0.67		
roads							
0 - 50	0.36					1.15	0.27
50 - 100	0.30					0.97	0.19
100 - 150	0.23					0.74	0.17
150 - 200	0.10					0.31	0.16
>200	0.02					0.06	0.13
Landcover		0.01	0.24	0.23	2.98		
Urban	0.17					1.48	0.17
Rocks	0.10					0.90	0.09
Arable	0.01					0.07	0.01
Permanent	0.10					0.92	0.13
cultivation							
Forest	0.11					0.95	0.11
Grassland	0.24					2.11	0.14
Shrubland	0.04					0.37	0.04
Sparse	0.12					1.08	0.21
vegetation							
Water body	0.12					1.05	0.09
TWI		0.17	0.25	0.08	1.00		
-2.12 - 1.52	0.19					1.01	0.20
1.52 - 3.35	0.20					1.04	0.20
3.35 - 5.70	0.18					0.92	0.18
5.70 - 9.62	0.17					0.90	0.18
9.62 - 20.06	0.25					1.30	0.24
TPI		0.00	0.31	0.31	1.35		
-1143.68 - -	0.00					0.00	0.00
202.34							
-202.34 - -	0.18					0.74	0.21
17.33							



-17.33 - -1.01	0.26				1.06	0.27
-1.01 - 20.75	0.24				0.98	0.26
20.75 - 243.84	0.31				1.24	0.27
TRI		0.00	0.34	0.34	1.47	
0 - 4.22	0.22				0.73	0.23
4.22 - 21.1	0.34				1.11	0.35
21.12 - 46.47	0.25				0.82	0.22
46.47 - 257.70	0.20				0.65	0.20
257.70 - 1077.30	0.00				0.00	0.00
Rainfall intensity		0.00	0.81	0.81	3.54	
84 - 110.83	0.81				11.29	0.32
110.83 - 127.38	0.08				1.15	0.27
127.38 - 140.80	0.05				0.70	0.15
140.80 - 157.35	0.06				0.81	0.19
157.35 - 198.05	0.00				0.00	0.06
NDVI		0.14	0.25	0.11	0.48	
-0.66 - 0.15	0.14				0.70	0.13
0.15 - 0.34	0.22				1.13	0.21
0.34 - 0.52	0.25				1.26	0.25
0.52 - 0.66	0.21				1.07	0.21
0.66 - 0.99	0.18				0.89	0.20
Aspect		0.05	0.15	0.09	0.41	
Flat (-1)	0.11				1.02	0.10
North (0-22.5)	0.08				0.75	0.07

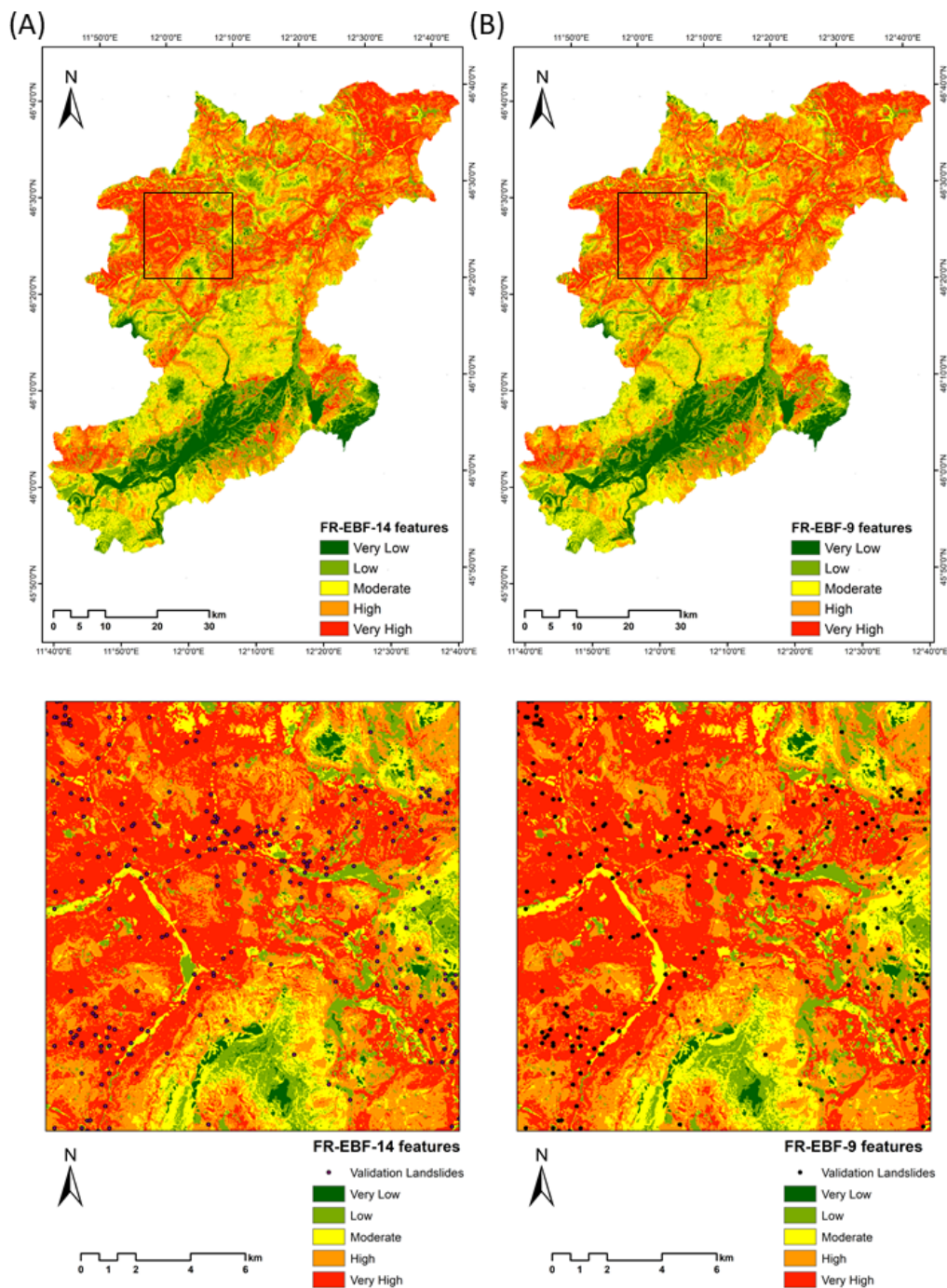


Northeast (22.5-67.5)	0.09				0.84	0.09
East (67.5- 112.5)	0.11				1.08	0.11
Southeast (112.5-157.5)	0.14				1.31	0.14
South (157.5- 202.5)	0.15				1.40	0.14
Southwest (202.5-247.5)	0.14				1.33	0.14
West (247.5- 292.5)	0.08				0.76	0.09
Northwest (292.5-337.5)	0.05				0.50	0.07
North (337.5- 360)	0.06				0.58	0.06
<hr/>						
Lithology		0.04	0.26	0.22	2.84	
Volcanites	0.26				3.45	0.16
Pre-Permian metamorphic sequence	0.11				1.50	0.11
Morainic	0.06				0.85	0.15
Gravels	0.04				0.52	0.04
Mix of alluvial deposits	0.05				0.70	0.03
Conglomerate	0.21				2.84	0.21

s



Limestone and dolomitic limestone	0.13	1.76	0.16
Calcareous shales	0.08	1.04	0.08
Shales and gypsums	0.06	0.76	0.07
Alternation of marls and sandstones	0.07	0.91	0.06
Water body	0.22	2.97	0.00





335 Figure 7: Landslide susceptibility maps derived using the ensemble of FR-EBF approaches
336 for (A) 14 landslide features and (B) 9 landslide features (Black square represents the
337 enlarged area).

338

339 4.2 Machine learning models

340 The LSM was generated based on the conditioning factor data, where the model learnt the
341 information from the feature maps, which helped identify areas of susceptibility. The final
342 results of the ML models in generating the LSM are given in Table 3. We observe that the AUC
343 scores of RF are not much apart from the XG-Boost model, indicating very good prediction
344 capability of both the models. Based on the information in Table 2, the number of pixels in the
345 moderate susceptibility class is more in the XG-Boost model than the RF model. Visually the
346 results show more susceptible areas near the landslide features (figures 8 and 9).

347 The model performance in terms of the accuracy of AUC is relatively similar to the results after
348 eliminating the lower degree of feature importance for both RF and XG-Boost. As discussed
349 previously in section 3.3, the feature importance for the ML models is carried out using the
350 impurity feature importance algorithm that enables to assess the relative relevance of the
351 conditioning factors in the optimal prediction of the landslides in terms of accuracy. As seen
352 in figure 10, the factors of Landcover, Profile Curvature, Plan Curvature, TWI and TPI have
353 the lowest values for the RF model. After trial-and-error, a value of 0.03 was chosen as the
354 threshold, and any factors above that were considered the "important" factors for landslide
355 susceptibility. Hence, in figure 8, we see that the five factors mentioned above are removed
356 and giving us 0.906 AUC as accuracy, which is better in AUC accuracy without removing the
357 five factors (0.902 Table 3).

358 Similarly, the same was repeated for the XG-Boost ML model and referring to Table 3, and
359 despite removing the lower valued conditioning factors of Profile Curvature, TPI, and Plan



360 Curvature, the AUC accuracy score was similar (Table 3). We observe that Slope and Distance
361 to Roads had a much bigger impact on the RF mode than the XG-Boost model. On the other
362 hand, Lithology played a bigger role in estimating landslide occurrences in the XG-Boost
363 model. These observations indicate interesting results which will be discussed further in the
364 discussion section.

365

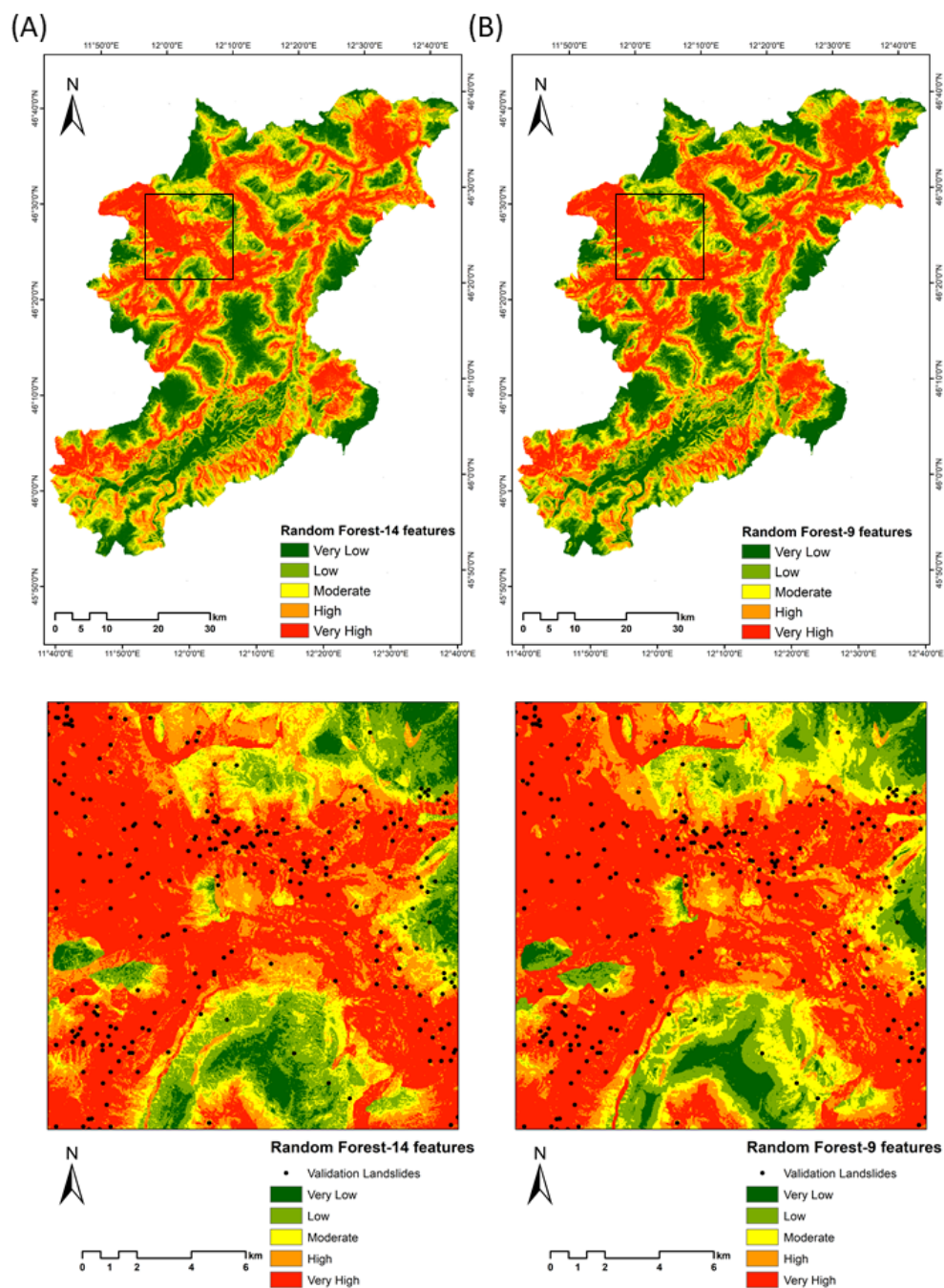
366 Table 3: Overall table with AUC results for landslide susceptibility of Belluno.

367

No.	Model	AUC
1	FR-EBF 14 features	0.836
2	FR-EBF 9 features	0.834
3	RF 14 features	0.902
4	RF 9 features	0.906
5	XG-Boost 14 features	0.910
6	XG-Boost 10 features	0.907

368

369



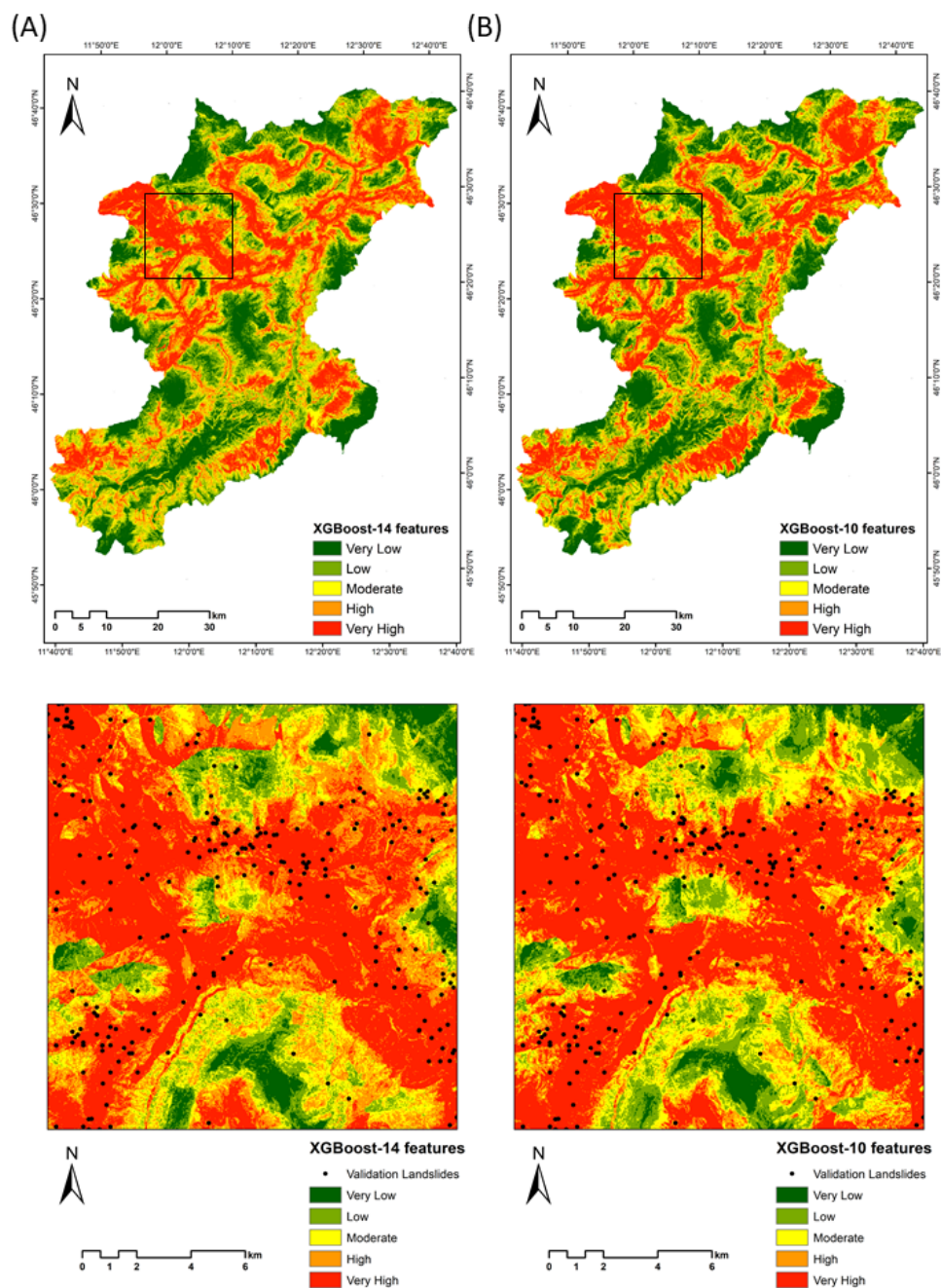


372 Figure 8: LSMs derived using the Random Forest approach for (A) 14 landslide features and

373 (B) 9 landslide features (Black square represents the enlarged area).

374

375



377

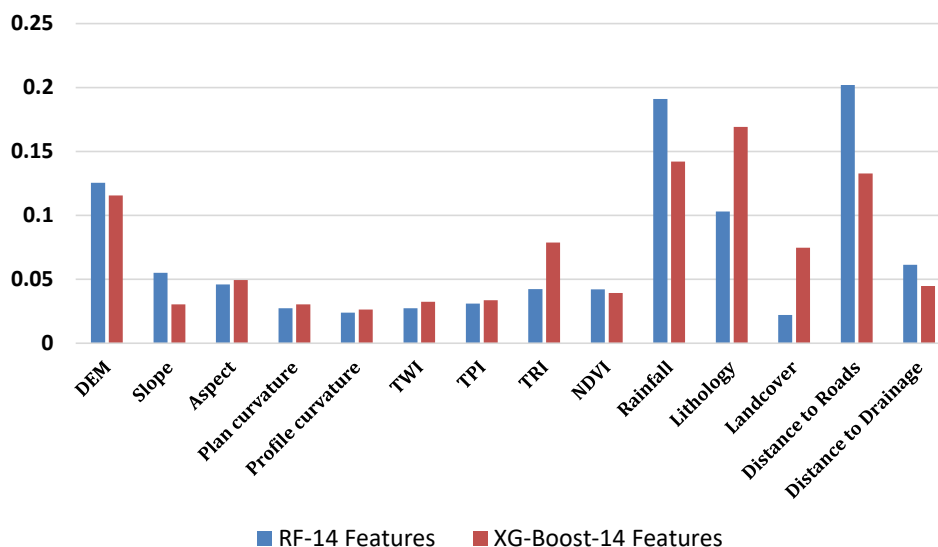
378

Figure 9: LSMs derived using the XG-Boost approach for



379 (A) 14 landslide features and (B) 9 landslide features (Black square represents the
380 enlarged area).

381



382

383

384 Figure 10: Feature importance of the RF and XG-Boost models.

385

386 5. Validation

387

388 Validation is crucial in producing quality LSMs for natural hazards where the information
389 presented in the map is beneficial for planners (Goetz et al., 2015) A number of validation
390 approaches may be used to assess the quality of the LSMs. We compare the landslide inventory
391 data to the resultant maps derived using the ensemble of FR-EBF, machine learning RF and
392 XG-Boost models. The efficiency of any model for LSM is calculated by comparing the
393 inventory data to the produced maps. This reflects if the models in use can accurately forecast
394 which areas are susceptible to landslides (Pourghasemi et al., 2018). The findings from the total



395 landslide input events were validated using 30% of the landslide occurrences. Validation for
396 this study was done using the Receiver Operating Characteristics (ROC) and the Relative
397 Landslide Density (R-Index) approaches.

398

399 5.1 Receiver Operating Characteristics (ROC)

400

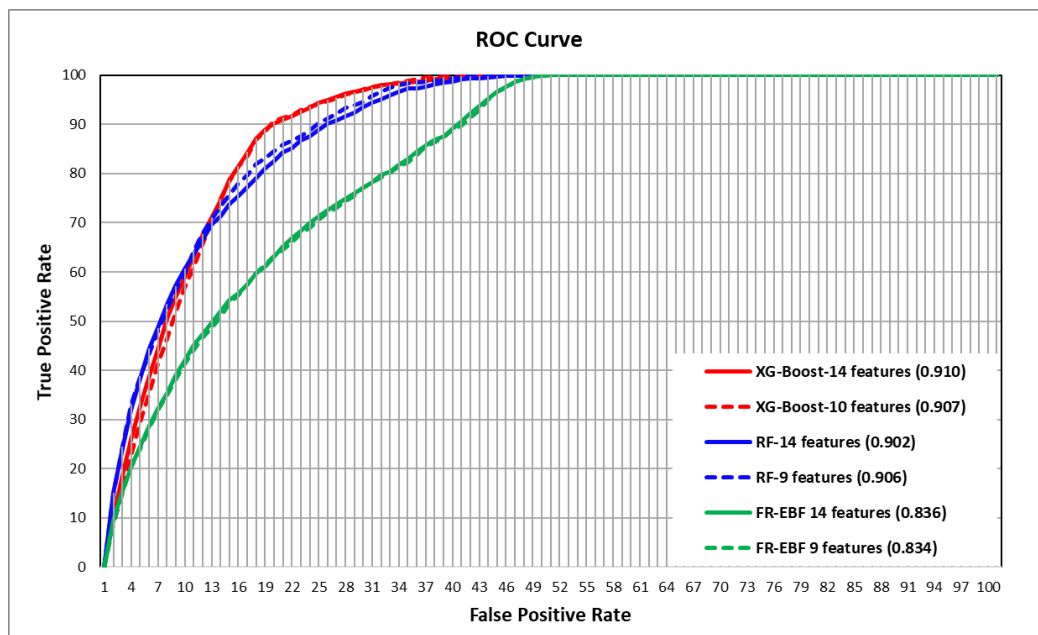
401 The receiver operating characteristics (ROC) approach was used for this study to corroborate
402 the six resultant LSMs from statistical and machine learning using the validation data. The
403 ROC approach demonstrates the assessment between the true positive rate (TPR) and the false
404 positive rate (FPR) in the resulting LSMs (Ghorbanzadeh et al., 2018; Linden, 2006). TPRs are
405 pixels in the landslide validation data that are correctly categorised as high susceptibility,
406 whereas FPRs are pixels that are erroneously labeled. TPRs versus FPRs are shown to create
407 ROC curves. The AUC refers to the degree to which the generated LSMs are accurate. The
408 AUC indicates whether more correctly labelled pixels were present than incorrectly labelled
409 pixels. Greater AUC values indicate that the susceptibility map is more accurate and the vice-
410 versa. If the AUC values are near to unity or one, the susceptibility map is meaningful. A map
411 with a value of 0.5 is considered insignificant since it was created by chance. (Baird, 2013).

412

413 Figure 11 shows the accuracy values obtained using the ROC technique for the statistical
414 approaches of FR-EBF and machine learning approaches of RF and XG-Boost. XG-Boost
415 shows the highest accurate results with an AUC value of 0.91 and RF with 0.906, and FR-EBF
416 with 0.836 (refer to Table 3). These results are quite good as it is closer to unity or one. The
417 ensemble of FR-EBF shows lower AUC values than the machine learning-based XG-Boost and
418 Random Forest. Machine learning results may vary as the models used landslides and non-
419 landslides features as training data, whereas results of FR-EBF are derived only from the



420 landslide data. The results could vary based on the geographical location and the selection of
421 landslide conditioning factors as well.



422

423

424 Figure 11. The ROC represents the success rate curves for the statistical based and machine
425 learning models for LSM in Belluno province, Italy.

426

427

428

429 5.2 Relative Landslide Density (R-Index)

430

431 The relative landslide density index was also used to assess the accuracy of the LSMs that
432 resulted (R-index). Equation (4) is used to get the R-index:

433

$$R = (n_i/N_i) / \sum(n_i/N_i) \times 100 \text{ (Eq.4)}$$

434



435 where N_i is the percentage of landslides in each susceptibility class and n_i is the percentage of
 436 land susceptible to landslides in each susceptibility class Table 4 shows the quantile
 437 classification approach to classify the six landslide susceptibility maps into five susceptible
 438 groups. In comparison to the RF and FR-EBF models, the XG-Boost model with 14 and 10
 439 features has a higher R-index for very high susceptibility classes. The R-index findings show
 440 that FR EBF has a better R-index value for high susceptibility class than XG-Boost, which has
 441 the lowest R-index for high susceptibility class. FR-EBF has a higher r-index value for the high
 442 susceptibility class than the other three approaches. In addition, the R-index of FR-EBF is
 443 higher for the very low susceptible class. Table 4 shows the R-index values for susceptibility
 444 class in FR-EBF, RF, and XG-Boost, as well as plots of the same in figure 12.

445

446 Table 4: R-indices for the FR-EBF, RF, and XG-Boost models' landslide susceptibility
 447 mappings (LSMs).

Validation methods	Susceptibility class	Number of pixels	Area (km ²)	Area (%) (ni)	Number of landslides	Landslide (%) (Ni)	R- index
FR-EBF-14							
Features	Very Low	21875	334248750	9.28	48	2.71	6
	Low	90000	570760000	15.85	171	9.66	13
	Moderate	165000	896709375	24.90	308	17.40	15
	High	263750	1026578125	28.50	460	25.99	20
	Very High	444375	773585000	21.48	783	44.24	45
FR-EBF-9							
Features	Very Low	19375	323332500	8.98	38	2.15	5
	Low	91875	541371875	15.03	179	10.11	15
	Moderate	153125	894758125	24.84	289	16.33	15
	High	276875	1041846875	28.93	480	27.12	21



	Very High	443750	800571875	22.23	784	44.29	44
RF-14							
Features	Very Low	6875	682346250	18.94	11	0.62	1
	Low	34375	658375000	18.28	55	3.11	4
	Moderate	75625	619031875	17.19	122	6.89	9
	High	159375	749470625	20.81	264	14.92	17
	Very high	712500	892657500	24.78	1318	74.46	69
RF-9							
Features	Very Low	7500	735246875	20.41	12	0.68	1
	Low	30000	632679375	17.57	48	2.71	4
	Moderate	75000	581844375	16.15	120	6.78	10
	High	147500	692276250	19.22	245	13.84	17
	Very High	729375	959834375	26.65	1345	75.99	68
XG-Boost-14							
Features	Very Low	11250	1076978750	29.90	18	1.02	1
	Low	6875	330045625	9.16	11	0.62	3
	Moderate	11875	278243750	7.72	19	1.07	5
	High	11250	352568125	9.79	18	1.02	4
	Very High	947500	1564045000	43.42	1704	96.27	87
	Very Low	12500	1094226250	30.38	20	1.13	1
	Low	7500	297782500	8.27	12	0.68	3
XG-Boost-10							
Features	Moderate	8125	242914375	6.74	13	0.73	4
	High	15625	314181875	8.72	25	1.41	7
	Very High	945000	1652776250	45.89	1700	96.05	84



449 Landslides are very dynamic in nature, meaning that their behaviour, movement, and spatial
450 distribution changes over space and time. Therefore, it is vital to analyse the significance of the
451 conditioning factors that lead to landslide occurrence. The relevance of the conditioning
452 features for LSM is essential to realize which of the features had impact on the prediction of
453 landslide occurrences. As not all features can be available globally, or even locally due to
454 various restriction or data unavailability, it is essential to choose the important features which
455 could be available for most use cases. For example, topographical features derived from digital
456 elevation models such as Elevation, Slope, aspect, Plan curvature, Profile curvature, TWI, TPI,
457 TRI. Other features, such as distance to roads and drainage networks, that might have direct or
458 indirect influence on the occurrence of landslides, can also be easily accessed through
459 numerous open-source platforms. In this study we used fourteen features for landslide
460 susceptibility assessment and carried out the feature importance test using traditional statistical
461 ensemble model of FR-EBF and machine learning models RF and XG-Boost. The feature
462 selection approach from statistical model is dependent upon the landslide data and its relation
463 to each feature and their classes. On the other hand, feature selection and determining their
464 importance using machine learning models depends upon the landslide and non-landslide
465 samples used to train the models. We used the in-built impurity feature importance algorithm
466 to assess the importance of the features during the model training phases. Based on literature
467 review for this sort of study, there is no standard threshold values available for discarding or
468 selection of features for LSM. In this study, we used a trial-and-error approach to determine a
469 threshold of 0.30 for selection of features used for landslide susceptibility for all the three
470 models.

471 Feature importance algorithms used in this study are different, however there is similarity in
472 the importance of the features in both statistical and machine learning algorithms (See figure 6
473 and 10). As we look at the figures 7, 8, and 9 in the enlarged region, we observe that there are



474 not many differences despite removing the least important features. The reason for such
475 observation can be linked to the lower impact of least important factors on overall LSM results.
476 Furthermore, there are several factors that determine the importance of features for carrying
477 out LSM such as (1) completeness and quality of the landslide inventory dataset used for
478 analysis, (2) mapping scale of the features maps like landcover, lithology, or other geological
479 features. If the spatial locations of landslides in an inventory does not represent the ground
480 truth phenomenon, then there can be negative impact of landslide input data for feature
481 selection. Most importantly, the type of landslide inventory data also impacts the landslide
482 feature selection algorithms, such as landslides mapped as points and polygons. Sampling
483 methodology of landslide selection is important, there are various ways to use landslides in
484 carrying out susceptibility assessment, many studies have used 70-30 ratio and others have
485 used random sampling or K-fold sampling methods (Chen et al., 2018; Merghadi et al., 2018).
486 One of the most important observations from this study was the reclusion of the "least important
487 features" in the context of LSM. The fact that despite removal of certain factors, we still get
488 very good results or comparable results post feature removal. This observation annotates the
489 use of very important features for LSM which can be obtained for most of the use cases.
490 The use of landslide samples along with non-landslide samples can affect the landslide feature
491 importance as can be seen in results in this study. In the case of the statistical model, one of the
492 reasons for the lower AUC performance can be accredited to the absence of the non-landslide
493 samples. Therefore, the model's ability to discriminate between the non-landslide and landslide
494 pixels is affected hence, predicting landslide occurrences over potentially non-landslide
495 locations. Thus, this exhibits the homogeneous distribution of predicted landslide pixels (see
496 figure 7). We used landslides and non-landslide samples for training the ML models which
497 shows varying results from that of the statistical ensemble model (See figure 8 and 9). There is
498 more homogeneous distribution of landslide susceptibility classes in statistical model results,



499 but it is evident from the machine learning results that the non-landslide samples have a greater
500 impact on final landslide susceptibility results.

501

502 7. Conclusions

503

504 In context of the current state-of-the-art approaches for LSM, the contemporary literature lays
505 emphasis on the advent of different models for improving accuracy of landslide occurrences
506 against the test data. However, this study investigated how the conditioning factors affect the
507 overall prediction of landslides in the context of northeast Italy, Belluno province. An
508 important aspect of this study was to identify if at all, removing the “least important”
509 conditioning factors in the modelling process affects the performance in predicting new
510 unknown landslides.

511 As understood, ML models require conditioning factors as input for LSM, however, investing
512 on the importance of the features (conditioning factors) could possibly direct a better
513 understanding of landslide occurrences with respect to the available factor/feature maps for
514 LSM. This study indicates that various models behave differently with different features,
515 whereby the same features that are important in one instance of a particular model, can be the
516 least important (even null-void) in other models. Therefore, this study gave new insights
517 towards the application and use of already available maps, without spending/exhausting
518 resources for generating other maps/features that would otherwise not be available, thus
519 suggesting a streamlined acquisition of data and modelling of landslide occurrences for future
520 events.

521 In this study we also concluded that the landslides and non-landslides samples impacts the
522 feature importance, especially in the ML models as these models use inputs in the form of
523 landslides and non-landslides samples. Therefore, it was found to be crucial in asserting a



524 balance between the two data samples to avoid overfitting or underfitting. This study illustrates
525 that feature selection is very important step of carrying out LSMs. We found that there are
526 differences in the final LSMs derived from the statistical and ML models, which are attributed
527 to the above-mentioned sample selection techniques.

528 This research introduces the importance of post-training feature importance algorithms for
529 LSM. This approach can also be used to assess the susceptibility of other natural disasters. The
530 results can eventually comment whether certain conditioning factors can be discarded while
531 modelling landslide occurrences. In many parts of the globe, the availability of data is scarce
532 and therefore, with the ability to model landslides without relying on the conventional factors,
533 we can still predict landslides spatially over a given region. Although there are certain
534 drawbacks like (1) the same factor maps will not be available everywhere, (2) factors that are
535 least important in one region might not repeat the same behaviour in other regions of the world,
536 and (3) model capability changes with respect to different regions, the resulting susceptibility
537 maps can still give quality information for local emergency relief measures, planning of disaster
538 risk reduction, mitigation, and to evaluate potentially affected areas.

539

540 Funding: This research was funded by the Veneto Region, VAIA-LANDslides project,
541 Research Unit UNIPD-GEO, Principal Investigator Mario Floris.

542

543

544 **References:**

545 Baglioni, A., Tosoni, D., De Marco, P., Arzilliero, L., 2006. Analisi del dissesto da frana in
546 Veneto.

547 Baird, C., 2013. Comparison of Risk Assessment Instruments in Juvenile Justice.



- 548 Boretto, G., Crema, S., Marchi, L., Monegato, G., Arzillero, L., Cavalli, M., 2021. Assessing
549 the effect of the Vaia storm on sediment source areas and connectivity storm in the Liera
550 catchment (Dolomites). Copernicus Meetings.
- 551 Brabb, E.E., Pampeyan, E.H., Bonilla, M.G., 1972. Landslide susceptibility in San Mateo
552 County, California, Miscellaneous Field Studies Map, Reston, VA.
- 553 Breiman, L., 2001. Random Forests. *Machine Learning* 45, 5-32.
- 554 Can, R., Kocaman, S., Gokceoglu, C., 2021. A Comprehensive Assessment of XGBoost
555 Algorithm for Landslide Susceptibility Mapping in the Upper Basin of Ataturk Dam, Turkey.
556 *Applied Sciences* 11, 4993.
- 557 Castellanos Abella, E.A., Van Westen, C.J., 2008. Qualitative landslide susceptibility
558 assessment by multicriteria analysis: A case study from San Antonio del Sur, Guantánamo,
559 Cuba. *Geomorphology* 94, 453-466.
- 560 Catani, F., Lagomarsino, D., Segoni, S., Tofani, V., 2013. Landslide susceptibility estimation
561 by random forests technique: sensitivity and scaling issues. *Natural Hazards and Earth
562 System Sciences* 13, 2815-2831.
- 563 Chacón, J., Irigaray, C., Fernández, T., El Hamdouni, R., 2006. Engineering geology maps:
564 landslides and geographical information systems. *Bulletin of Engineering Geology and the
565 Environment* 65, 341-411.
- 566 Chen, T., Trinder, J.C., Niu, R., 2017. Object-oriented landslide mapping using ZY-3 satellite
567 imagery, random forest and mathematical morphology, for the Three-Gorges Reservoir,
568 China. *Remote sensing* 9, 333.
- 569 Chen, W., Peng, J.B., Hong, H.Y., Shahabi, H., Pradhan, B., Liu, J.Z., Zhu, A.X., Pei, X.J.,
570 Duan, Z., 2018. Landslide susceptibility modelling using GIS-based machine learning
571 techniques for Chongren County, Jiangxi Province, China. *Science of the Total Environment*
572 626, 1121-1135.
- 573 Chung, C.-J.F., Fabbri, A.G., 2003. Validation of Spatial Prediction Models for Landslide
574 Hazard Mapping. *Natural Hazards* 30, 451-472.



- 575 Compagnoni, B., Galluzzo, F., Bonomo, R., Tacchia, D., 2005. Carta geologica d'Italia.
576 Dipartimento difesa del suolo.
- 577 Corò, D., Galgaro, A., Fontana, A., Carton, A., 2015. A regional rockfall database: the Eastern
578 Alps test site. *Environmental Earth Sciences* 74, 1731-1742.
- 579 Dahal, R.K., Hasegawa, S., Nonomura, A., Yamanaka, M., Masuda, T., Nishino, K., 2008.
580 GIS-based weights-of-evidence modelling of rainfall-induced landslides in small catchments
581 for landslide susceptibility mapping. *Environmental Geology* 54, 311-324.
- 582 Dai, F.C., Lee, C.F., Ngai, Y.Y., 2002. Landslide risk assessment and management: an
583 overview. *Engineering Geology* 64, 65-87.
- 584 Desiato, F., Lena, F., Baffo, F., Suatoni, B., Toreti, A., di Ecologia Agraria, U.C., Romagna,
585 A.E., 2005. Indicatori del clima in Italia. APAT, Roma.
- 586 Doglioni, C., 1990. Thrust tectonics examples from the Venetian Alps.
- 587 Dunning, S., Massey, C., Rosser, N., 2009. Structural and geomorphological features of
588 landslides in the Bhutan Himalaya derived from terrestrial laser scanning. *Geomorphology*
589 103, 17-29.
- 590 Dury, G., 1972. Hillslope form and Process. M.A. Carson and M.J. Kirkby, 1972. Cambridge
591 University Press, London, vii + 475 pp., £ 6.60.
- 592 Ercanoglu, M., Gokceoglu, C., 2002. Assessment of landslide susceptibility for a landslide-
593 prone area (north of Yenice, NW Turkey) by fuzzy approach. *Environmental Geology* 41, 720-
594 730.
- 595 Floris, M., Iafelice, M., Squarzone, C., Zorzi, L., De Agostini, A., Genevois, R., 2011. Using
596 online databases for landslide susceptibility assessment: an example from the Veneto Region
597 (northeastern Italy). *Nat. Hazards Earth Syst. Sci.* 11, 1915-1925.
- 598 Gariano, S.L., Verini Supplizi, G., Ardizzone, F., Salvati, P., Bianchi, C., Morbidelli, R.,
599 Saltalippi, C., 2021. Long-term analysis of rainfall-induced landslides in Umbria, central Italy.
600 *Natural Hazards* 106, 2207-2225.
- 601 Ghorbanzadeh, O., Rostamzadeh, H., Blaschke, T., Gholaminia, K., Aryal, J., 2018. A new
602 GIS-based data mining technique using an adaptive neuro-fuzzy inference system (ANFIS)



603 and k-fold cross-validation approach for land subsidence susceptibility mapping. *Natural*
604 *Hazards* 94, 497-517.

605 Glade, T., Anderson, M.G., Crozier, M.J., 2006. *Landslide hazard and risk*. John Wiley & Sons.

606 Goetz, J.N., Brenning, A., Petschko, H., Leopold, P., 2015. Evaluating machine learning and
607 statistical prediction techniques for landslide susceptibility modeling. *Computers &*
608 *Geosciences* 81, 1-11.

609 Guzzetti, F., Reichenbach, P., Ardizzone, F., Cardinali, M., Galli, M., 2006. Estimating the
610 quality of landslide susceptibility models. *Geomorphology* 81, 166-184.

611 Huang, F., Chen, J., Du, Z., Yao, C., Huang, J., Jiang, Q., Chang, Z., Li, S., 2020. Landslide
612 Susceptibility Prediction Considering Regional Soil Erosion Based on Machine-Learning
613 Models. *ISPRS International Journal of Geo-Information* 9, 377.

614 Iadanza, C., Trigila, A., Starace, P., Dragoni, A., Biondo, T., Roccisano, M., 2021. IdroGEO:
615 A Collaborative Web Mapping Application Based on REST API Services and Open Data on
616 Landslides and Floods in Italy. *ISPRS International Journal of Geo-Information* 10, 89.

617 Komac, M., 2006. A landslide susceptibility model using the Analytical Hierarchy Process
618 method and multivariate statistics in perialpine Slovenia. *Geomorphology* 74, 17-28.

619 Linden, A., 2006. Measuring diagnostic and predictive accuracy in disease management: an
620 introduction to receiver operating characteristic (ROC) analysis. *Journal of evaluation in*
621 *clinical practice* 12, 132-139.

622 Liu, L.-L., Yang, C., Wang, X.-M., 2021. Landslide susceptibility assessment using feature
623 selection-based machine learning models. *Geomechanics and Engineering* 25, 1-16.

624 Melville, B., Lucieer, A., Aryal, J., 2018. Object-based random forest classification of Landsat
625 ETM+ and WorldView-2 satellite imagery for mapping lowland native grassland communities
626 in Tasmania, Australia. *International journal of applied earth observation and geoinformation*
627 66, 46-55.

628 Merghadi, A., Abderrahmane, B., Tien Bui, D., 2018. Landslide Susceptibility Assessment at
629 Mila Basin (Algeria): A Comparative Assessment of Prediction Capability of Advanced
630 Machine Learning Methods. *ISPRS International Journal of Geo-Information* 7.



- 631 Meten, M., PrakashBhandary, N., Yatabe, R., 2015. Effect of Landslide Factor Combinations
632 on the Prediction Accuracy of Landslide Susceptibility Maps in the Blue Nile Gorge of Central
633 Ethiopia. *Geoenvironmental Disasters* 2, 9.
- 634 Micheletti, N., Foresti, L., Robert, S., Leuenberger, M., Pedrazzini, A., Jaboyedoff, M.,
635 Kanevski, M., 2014. Machine Learning Feature Selection Methods for Landslide Susceptibility
636 Mapping. *Mathematical Geosciences* 46, 33-57.
- 637 Pham, B.T., Tien Bui, D., Pourghasemi, H.R., Indra, P., Dholakia, M.B., 2015. Landslide
638 susceptibility assessment in the Uttarakhand area (India) using GIS: a comparison study of
639 prediction capability of naïve bayes, multilayer perceptron neural networks, and functional
640 trees methods. *Theoretical and Applied Climatology* 128, 255-273.
- 641 Pham, B.T., Tien Bui, D., Prakash, I., 2018. Bagging based Support Vector Machines for
642 spatial prediction of landslides. *Environmental Earth Sciences* 77, 146.
- 643 Pourghasemi, H.R., Gayen, A., Park, S., Lee, C.W., Lee, S., 2018. Assessment of Landslide-
644 Prone Areas and Their Zonation Using Logistic Regression, LogitBoost, and NaiveBayes
645 Machine-Learning Algorithms. *Sustainability* 10.
- 646 Pourghasemi, H.R., Pradhan, B., Gokceoglu, C., 2012. Application of fuzzy logic and analytical
647 hierarchy process (AHP) to landslide susceptibility mapping at Haraz watershed, Iran. *Natural*
648 *Hazards* 63, 965-996.
- 649 Pradhan, B., 2010. Landslide susceptibility mapping of a catchment area using frequency
650 ratio, fuzzy logic and multivariate logistic regression approaches. *Journal of the Indian Society*
651 *of Remote Sensing* 38, 301-320.
- 652 Raja, N.B., Çiçek, I., Türkoğlu, N., Aydin, O., Kawasaki, A., 2017. Landslide susceptibility
653 mapping of the Sera River Basin using logistic regression model. *Natural Hazards* 85, 1323-
654 1346.
- 655 Reichenbach, P., Rossi, M., Malamud, B.D., Mihir, M., Guzzetti, F., 2018. A review of
656 statistically-based landslide susceptibility models. *Earth-Science Reviews* 180, 60-91.
- 657 Riley, S.J., DeGloria, S.D., Elliot, R., 1999. Index that quantifies topographic heterogeneity.
658 *intermountain Journal of sciences* 5, 23-27.



- 659 Rossi, M., Guzzetti, F., Salvati, P., Donnini, M., Napolitano, E., Bianchi, C., 2019. A predictive
660 model of societal landslide risk in Italy. *Earth-Science Reviews* 196, 102849.
- 661 Sahin, E.K., 2020. Assessing the predictive capability of ensemble tree methods for landslide
662 susceptibility mapping using XGBoost, gradient boosting machine, and random forest. *SN*
663 *Applied Sciences* 2, 1308.
- 664 Sauro, F., Zampieri, D., Filipponi, M., 2013. Development of a deep karst system within a
665 transpressional structure of the Dolomites in north-east Italy. *Geomorphology* 184, 51-63.
- 666 Schönborn, G., 1999. Balancing cross sections with kinematic constraints: The Dolomites
667 (northern Italy). *Tectonics* 18, 527-545.
- 668 Senouci, R., Taibi, N.-E., Teodoro, A.C., Duarte, L., Mansour, H., Yahia Meddah, R., 2021.
669 GIS-Based Expert Knowledge for Landslide Susceptibility Mapping (LSM): Case of
670 Mostaganem Coast District, West of Algeria. *Sustainability* 13, 630.
- 671 Shahabi, H., Hashim, M., 2015. Landslide susceptibility mapping using GIS-based statistical
672 models and Remote sensing data in tropical environment. *Scientific reports* 5, 9899.
- 673 Stanley, T.A., Kirschbaum, D.B., Benz, G., Emberson, R.A., Amatya, P.M., Medwedeff, W.,
674 Clark, M.K., 2021. Data-Driven Landslide Nowcasting at the Global Scale. *Frontiers in Earth*
675 *Science* 9.
- 676 Trigila, A., Iadanza, C., 2018. Landslides and floods in Italy: hazard and risk indicators -
677 Summary Report 2018.
- 678 Trigila, A., Iadanza, C., Spizzichino, D., 2010. Quality assessment of the Italian Landslide
679 Inventory using GIS processing. *Landslides* 7, 455-470.
- 680 van Westen, C.J., Castellanos, E., Kuriakose, S.L., 2008. Spatial data for landslide
681 susceptibility, hazard, and vulnerability assessment: An overview. *Engineering Geology* 102,
682 112-131.
- 683 Youssef, A.M., Pourghasemi, H.R., 2021. Landslide susceptibility mapping using machine
684 learning algorithms and comparison of their performance at Abha Basin, Asir Region, Saudi
685 Arabia. *Geoscience Frontiers* 12, 639-655.
- 686